APPLIED SCIENCES AND ENGINEERING

Closed-loop additive manufacturing of upcycled commodity plastic through dynamic cross-linking

Sungjin Kim[1], Md Anisur Rahman[1], Md Arifuzzaman[1], Dustin B. Gilmer[2], Bingrui Li[2], Jackson K. Wilt[1], Edgar Lara-Curzio[3], Tomonori Saito[1]*

A sustainable closed-loop manufacturing would become reality if commodity plastics can be upcycled into higher-performance materials with facile processability. Such circularity will be realized when the upcycled plastics can be (re)processed into custom-designed structures through energy/resource-efficient additive manufacturing methods, especially by approachable and scalable fused filament fabrication (FFF). Here, we introduce a circular model epitomized by upcycling a prominent thermoplastic, acrylonitrile butadiene styrene (ABS) into a recyclable, robust adaptive dynamic covalent network (ABS-vitrimer) (re)printable via FFF. The full FFF processing of ABS-vitrimer overcomes the major challenge of (re)printing cross-linked materials and produces stronger, tougher, solvent-resistant three-dimensional objects directly reprintable and separable from unsorted plastic waste. This study thus offers an imminently adoptable approach for advanced manufacturing toward the circular plastics economy.

INTRODUCTION

Plastics production [currently >400 (megaton) Mt/year] and incineration are estimated to account for 16% of the global net carbon emission by 2050—a significant surge from 2.3% in 2013 (*1*–*5*). Integrative interventions, including increasing the plastics recycling rate and reducing the production demand growth, were simulated to reduce carbon dioxide (CO_2) emissions by 93% in the best-case scenario (*6*). Thus, establishing the closed-loop circularity of plastics is crucial for achieving net-zero carbon emission (*7*, *8*). For example, recycling polydiketoenamines with a circular design was reported to emit only $^1/_{43}$ of CO_2 compared with producing virgin resins without circularity (*5*). However, the recycling rate of traditional plastics remains low because of the deteriorating properties of plastics upon recycling and added costs (*9*). Therefore, developing manufacturing paths of plastics with circularity in value-enhancing manners is a key enabler toward establishing net-zero carbon emissions.

Among manufacturing technologies, additive manufacturing (AM) provides on-demand bottom-up three-dimensional (3D) material production, which can reduce energy use by 25% and materials' waste and costs by up to 90% from traditional manufacturing methods (*10*, *11*). Therefore, if plastic wastes can be turned into useful 3D structures with better material performance through AM in simple and scalable manners, then such an upcycling approach can change the paradigm for the circular plastics economy (*9*, *12*). In this respect, fused filament fabrication (FFF) is the most accessible and user-friendly AM technology and comprised 69% of the global 3D printing market share in 2018, thanks to the approachable printing protocols of layer-by-layer deposition by extruded fused polymer filaments (*13*–*15*). FFF is also scalable to build industry-scale automotive, building, or aircraft parts demonstrated by the Big Area Additive Manufacturing system (*16*). However, the prerequisite of FFF for materials to be extrudable and printable typically excludes the cross-linked thermosets despite their advantages in the thermomechanical and chemical stabilities (Fig. 1A). Thus, typical polymers used in FFF have been limited to thermoplastics such as acrylonitrile butadiene styrene (ABS), poly(lactic acid), poly(carbonate), or poly(ethylene terephthalate), which have appropriate viscoelasticity for extrusion deposition and proper mechanical strength before and after printing. Among them, ABS (produced 11.17 Mt/year, 2018) is one of the most widely used FFF-printable polymers with wide-ranging applications from auto parts to table tennis balls and LEGO blocks, owing to its thermomechanical toughness, rigidity, and cost-effectiveness (*17*). If discarded commodity thermoplastics like ABS can be upcycled into materials with enhanced mechanical-chemical properties and (re)printability in desired 3D structures, such a strategy can epitomize transformative manufacturing toward better sustainability.

We hereby open a circular upcycling of a commodity plastic exemplified by ABS into a higher-performance vitrimer with full FFF (re)processability in conventional printing conditions and robust printout properties comparable to cross-linked thermosets (Fig. 1B). Vitrimer exhibits mechanical robustness and chemical resistance because of its covalent network formation, but it can also be malleable by reconfiguring reversible cross-links through the associative bond exchange at elevated temperature, making it recyclable (Fig. 1A) (*18*–*20*). Recently, Smaldone and co-workers (*21*–*23*) developed FFF-printable thermosets based on dissociative Diels-Alder bonds that break to depolymerize at high temperature for extrusion followed by repolymerization upon cooling to enhance the interlayer bonding in the printout. For soft networks like elastomers or gels (*24*–*26*), another extrusion AM method such as direct ink writing (DIW) has been used for printing cross-linked thermosets with the presence of dynamic bonds; however, reprinting the strong, robust network by DIW is limited without chemical or thermal depolymerization (*27*). While the previously reported studies shed light on printing cross-linked networks with reversible bonds, a different approach needs to be developed for upcycling commodity plastics and their (re)printing. To design the ABS upcycled to a vitrimer system (labeled as ABS-vitrimer) directly (re)printable in typical FFF conditions, we used associative imine exchange, which has been applied to develop recyclable vitrimers (*28*–*34*). In particular,

[1]Chemical Sciences Division, Oak Ridge National Laboratory, Oak Ridge, TN 37831, USA. [2]Bredesen Center for Interdisciplinary Research and Graduate Education, University of Tennessee, Knoxville, TN 37996, USA. [3]Materials Sciences and Technology Division, Oak Ridge National Laboratory, Oak Ridge, TN 37831, USA.
*Corresponding author. Email: saitot@ornl.gov

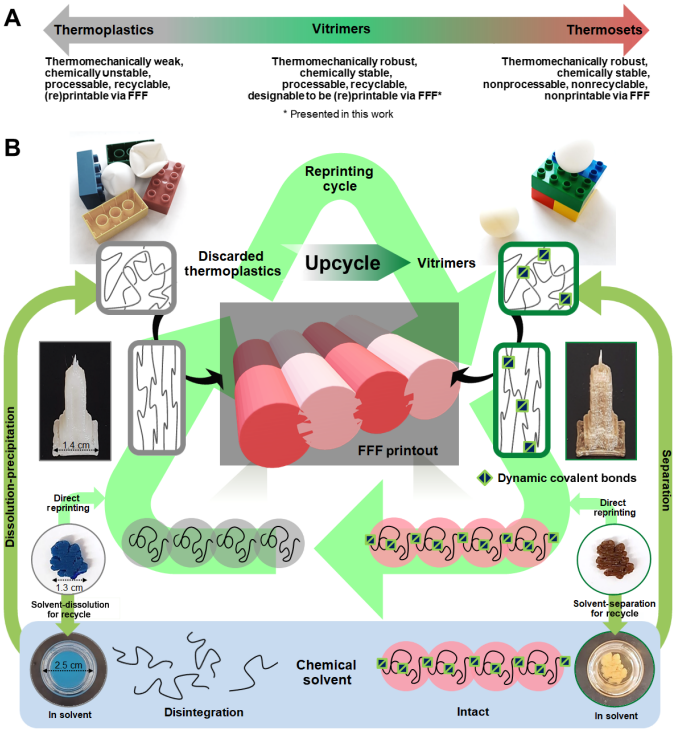

Fig. 1. Circular model design of upcycling thermoplastics into recyclable vitrimer for FFF. (**A**) Schematic diagram comparing characteristics of traditional thermoplastics, thermosets, and vitrimers. (**B**) Schematic illustration of the circular design of upcycling thermoplastics to FFF-(re)printable vitrimer. Dynamic covalent cross-links in the vitrimer readily rearranged to enable FFF (re)printing at high temperature while enhancing interfilament strength and solvent stability of printouts. The photographs show structures printed from the untreated ABS (Neat-ABS) (left) and the ABS-vitrimer (right) of a building (top) and an oak leaf before (middle) and after (bottom) immersion in tetrahydrofuran (THF) for 48 hours. The ABS-vitrimer preserved its structure, whereas the Neat-ABS completely dissolved. Thus, ABS-vitrimer and Neat-ABS can be recycled through separation and dissolution-precipitation, respectively, from their waste mixture solution, wherefrom the dissolved Neat-ABS can be re-upcycled into ABS-vitrimer (detailed discussion in a later section).

we gave attention to the high apparent activation energy ($E_a \approx 150$ kJ/mol) of transimination among many associative exchange reactions (*35*), which can be advantageous for FFF printability upon rapid heating at the printhead (more discussion in later sections).

Our approach of upcycling ABS into ABS-vitrimer proved notable improvements in thermomechanical and chemical robustness and maintained facile printability by FFF, overcoming the major challenge of (re)printing cross-linked materials. We also postulated that the associative bond exchange between the vitrimer layers upon printing could improve the inherently weak interfilament bonding and solvent resistance of the FFF-printed structures (*13*, *35*–*37*) without stepwise depolymerization-repolymerization or postextrusion cross-linking. In addition, the ABS-vitrimer demonstrated the multipath recyclability wherein the ABS-vitrimer wastes could be easily separated from mixtures with other plastics by dissolution or directly reprinted through FFF into useful 3D structures, and the dissolved unmodified ABS can be again upcycled to ABS-vitrimers (Fig. 1B). Thus, this value-enhancing cycle is expected to reduce the CO_2-equivalent emissions by at least 65% expected from simple dissolution-precipitation recycles compared to incineration (*38*). Full FFF processing of cross-linked materials including vitrimers is rarely demonstrated, and thus, the ABS-vitrimer convertible from discarded wastes to feedstock filaments and then to desired 3D structures provides unique advantages distinguished from other mechanical or chemical recycling methods. The FFF of upcycled ABS-vitrimers thus introduces a readily adoptable approach to fulfill the intertwined thermomechanical-chemical-environmental needs for circular plastics manufacturing (more detailed background is available in Supplementary Text).

RESULTS

Our strategy used one-step modification to upcycle the ABS to an FFF-printable vitrimer. In ABS, rubbery butadiene segments provide ductility and toughness and importantly contain the unsaturated double bonds amenable for postfunctionalization (*17*). We implemented thiol-ene "click" chemistry (*39*, *40*) to functionalize butadiene segments with cysteamine, followed by reacting with a short-chain dialdehyde (i.e., glutaraldehyde) to produce ABS-vitrimer (see Materials and Methods for details). Both cysteamine and glutaraldehyde are widely available U.S. Food and Drug Administration/World Health Organization–enlisted compounds: The former is biosynthesized in humans and used as eyedrops for cystinosis, and the latter is a disinfectant (table S1). We modified the virgin ABS [(A):(B):(S) = 18:18:64 mole percent (mol %)] or its discarded waste to attach primary amine groups via the thiol-ene click reaction of cysteamine on butadiene groups in ABS (Fig. 2A and fig. S1). The reaction mixture visibly turned from a colorless solution into pale lime–yellow solution. The ^{1}H nuclear magnetic resonance (NMR) results confirmed that the original 18 mol % of butadiene segments in ABS were reduced to 4 mol %, along with the corresponding increase of aminoethyl thioether, indicating that 14 mol % of the segments are attached with primary amines (fig. S2). Subsequently, the amine-modified ABS underwent imine formation with the glutaraldehyde cross-linker (Fig. 2B) in varied ratios (i.e., indicated by ALD-XX, where XX% = [—CHO]/[—NH_2]). The reaction mixture turned orange pink in different saturations according to aldehyde concentrations, followed by curing at 150°C for further transimination. The imine cross-linking is evidenced by the Fourier transform infrared (FTIR) spectroscopy (fig. S3), solid-state ^{13}C NMR (fig. S4), and solvent resistance (*35*, *36*) in multiple solvents, including tetrahydrofuran (THF), acetone, chloroform, dichloromethane (DCM), and dimethylformamide (DMF) (fig. S6) (*41*). The change of T_g (~118° ± 1°C) or thermal stability upon cross-linking was insignificant, indicating the preservation of thermal processability of ABS (table S2 and fig. S5).

Mechanical properties of ALD-0, ALD-08, ALD-17, ALD-33, ALD-66, and ALD-124 were assessed by tensile tests and compared with untreated ABS (labeled as Neat-ABS) (Fig. 2C). The functionalization of ductile butadiene segments via the thiol-ene reaction (*17*) reduced the overall toughness of ABS, as seen from ALD-0. Adjusting the fraction of ALD cross-linkers—ALD-08, ALD-17, and ALD-33—controllably improved the strength and toughness, likely because the partial cross-linking connected individual chains to increase effective overall polymer chain structures responding to the external force, which allows chains to be held together longer upon crazing against tensile fracture (fig. S7). Compared with the ~3.8 MJ/m^3 toughness and the ~25 MPa ultimate tensile strength (UTS) of the Neat-ABS (*37*, *42*), the ALD-33 nearly doubled the toughness

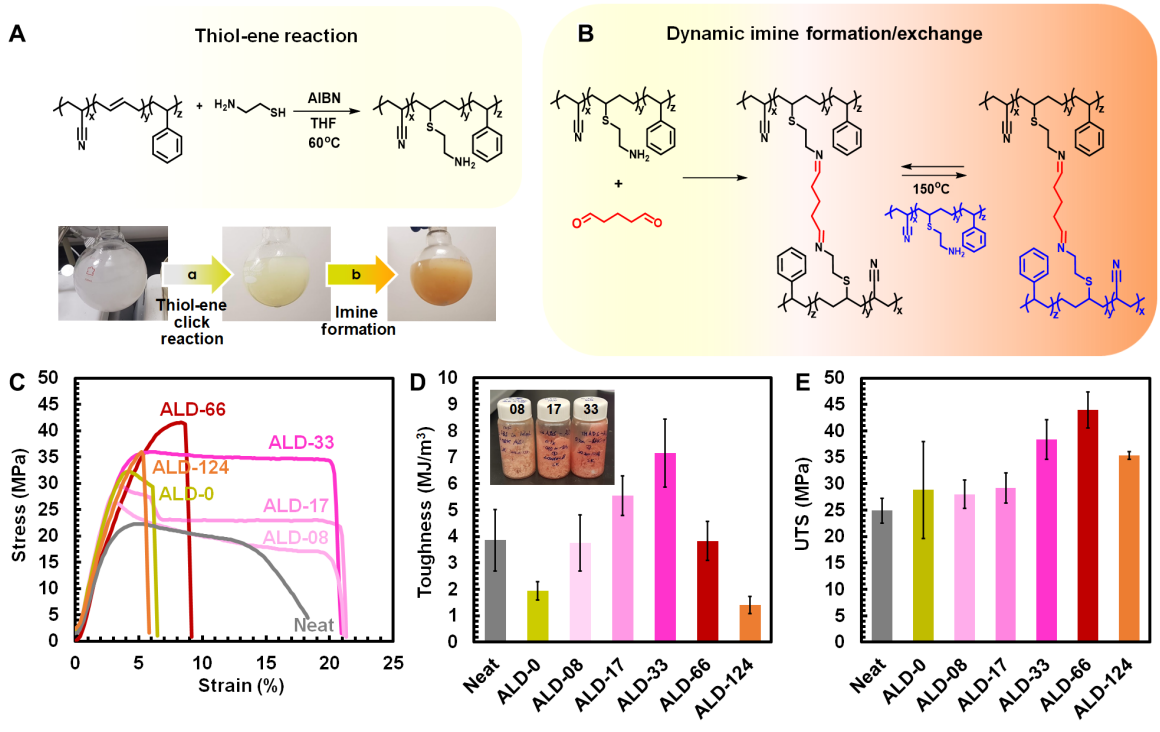

Fig. 2. Chemical upcycling pathway to synthesize ABS with dynamic imine cross-links and their tailored mechanical properties. (**A**) The Neat-ABS was modified to contain amine groups via thiol-ene reaction of cysteamine with butadiene groups at 60°C by using azobisisobutyronitrile (AIBN) as the initiator. (**B**) The modified ABS underwent the imine formation reaction with glutaraldehyde in the solution state, dried, and then cured at 150°C. (**C**) Tensile stress-strain curves of Neat, ALD-0, ALD-08, ALD-17, ALD-33, ALD-66, and ALD-124. Comparison of (**D**) toughness (inset is a photo of synthesized ALD-08, ALD-17, and ALD-33 samples with different color saturations) and (**E**) UTS of the specimens in (C). The error bars indicate SDs from at least triplicate measurements.

to ~7.2 MJ/m^3 and increased the UTS by 54% to ~38 MPa (Fig. 2, D and E, and table S3). When the network was cross-linked with excessive cross-linkers (i.e., ALD-124), the plasticity was lost, implying that the chain movement beyond the elastic regime was restricted by denser covalent cross-links (fig. S7). The UTS of ALD-66 reached ~44 MPa, which is >80% increase from the Neat-ABS, but the trade-off in deformability was likewise attributed to the denser network. Thus, ALD-33 was selected as the primary formulation to represent the imine–cross-linked system for printing and other investigations because toughness and ductility are desirable for fracture-free preprinting steps and printout properties.

The viscoelastic properties and processabilities were examined at temperatures higher than T_g by rheometry on hot-pressed vitrimer films (Fig. 3A). The rheological master curve (Fig. 3B and table S4) shows that ALD-33 exhibits more solid-like behavior evidenced by twofold higher G' (storage modulus) and slower terminal relaxation than Neat-ABS at $\omega \approx 1$ rad/s. In addition, the stress-relaxation test was performed to find relaxation times (τ) and their Arrhenius behavior, which is widely reported for vitrimers (see Materials and Methods for details). Within 100 s, the τ of ALD-33 could be determined for all measured temperatures, and complete relaxation was observed at 170°C within 1000 s (fig. S8), indicating that cross-links in the network were exchangeable. The temperature dependence of τ for ALD-33 showed good agreement with Arrhenius law (Fig. 3C and table S5), resulting in $E_a \approx 151$ kJ/mol, which is consistent with previously reported value (~157 kJ/mol) for polyimine vitrimers (*28*, *35*). In contrast, the Neat-ABS poorly followed the Arrhenius relation, and its obtained τ was consistently shorter than that of ALD-33 in all measured temperatures (fig. S9 and table S6). Creep tests further demonstrated superior thermomechanical stability and Arrhenius behavior of the ABS-vitrimer (figs. S10 and S11 and table S7). On the basis of these results, the hypothetical topology freezing transition temperature (T_v) was estimated to be ~54°C (fig. S9 and table S8) (*43*). The T_v is considered as the temperature above which the dynamic exchange can occur and can be estimated from the extrapolation of the Arrhenius plot (details in table S8) (*44*). Therefore, the dynamic transimination should readily occur in the tested temperature range of 130° to 170°C. The E_a of ALD-33 (~151 kJ/mol) is high among reported vitrimer systems (*35*), indicating that the system becomes rapidly dynamic upon temperature increase toward the extrusion temperature of ~230°C to facilitate processing while improving thermomechanical stability near T_g.

The recyclability of ALD-33 was evaluated using dynamic mechanical analysis (DMA) (Fig. 3, D and E, and fig. S12) and tensile tests (table S9) on samples fractured from the pristine film and then repressed at 150°C to reproduce the film up to three cycles (re 1 to 3) (Fig. 3A). The DMA profiles of the four samples showed nearly identical storage moduli (E') upon three recycles, indicating a good recovery of its elasticity (Fig. 3D). Correspondingly, the T_g determined by the DMA tan δ peak showed insignificant change throughout three recycles, confirming no considerable alteration in elasticity and processability (Fig. 3E). The tensile tests on these samples also displayed a good recovery of the UTS and ductility (table S9). This conservation of network elasticity suggests that the dynamic covalent cross-links were restorable during reprocessing cycles. Thus, the observed reprocessability proves that the cross-linked ABS-vitrimer

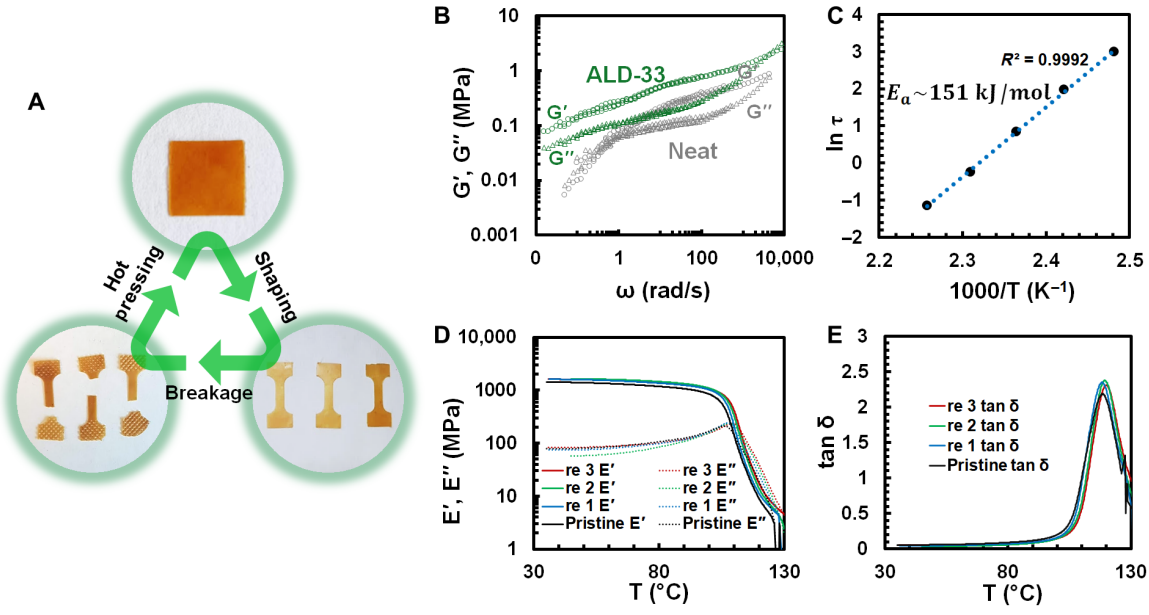

Fig. 3. Processability and viscoelastic behavior of ABS-vitrimer. (**A**) Schematics describing the (re)processability of ALD-33. ALD-33 could be hot-pressed into a film at 150°C, shaped as desired, broken apart, and repressed into a film at 150°C. (**B**) Rheological behavior at 150°C of Neat-ABS and ALD-33 characterized by frequency sweep at 1% strain from small-angle oscillatory shear test and time-temperature superposition (measured 130° to 170°C with 10°C intervals, reference T = 150°C). (**C**) Arrhenius relation from obtained relaxation time (τ) from stress-relaxation profiles of ALD-33 (fig. S8). The deduced E_a is ~151 kJ/mol (see Materials and Methods and table S5 for more details). (**D**) Dynamic mechanical analysis (DMA) of ALD-33 films upon three recycles (re 1 to 3) in oscillation temperature increase from 35° to 130°C (amplitude, 20 μm; frequency, 1 Hz; T ramp rate, 3°C/min). Note that meaningful measurements above 130°C were unavailable using our apparatus configurations because of sample deformation of ABS systems (fig. S12). (**E**) The loss factor (tan δ = E''/E') recorded via the measurement in (D).

can be recycled by reheating without solvents or additives to dissociate the network, enabling (re)printability by heating in FFF protocols.

The key to the direct FFF printability of vitrimer is imparting fast exchange kinetics and malleability with mechanical integrity for self-standing structure during printing. We established a system (i.e., ALD-33) with a good balance between strength and deformability (Fig. 2, C to E) and, importantly, the free $-NH_2$ groups sufficiently available for facile imine bond exchange with cross-linkers (Figs. 2, B to E, and 3, B and C). The τ of ALD-33 approaches that of Neat-ABS above 170°C (tables S5 and S6) and becomes as short as 0.002 s at the typical ABS-printing temperature of 230°C (extrapolated from Arrhenius plot in Fig. 3C). On the basis of such fast bond exchange and good processability, the ABS-vitrimer was successfully printed in common FFF protocols for Neat-ABS involving the feedstock filament extrusion (fig. S13), loading, feeding, and printing without any postprocessing (see Materials and Methods for details). Dog-bone specimens (fig. S14) were printed with transverse (Fig. 4, A to C) and longitudinal (Fig. 4, D to F) infill patterns. The tensile strength of transverse-printed specimens thus represents the interlayer strength because layer joints intrinsically make topological valleys where tensile stress concentrates (*37*). The ALD-33 exhibits ~1.6 times higher strength in both printing patterns. Notably, the interlayer strength of Neat-ABS (~15 MPa) improved to ~25 MPa in ALD-33 by incorporating the dynamic imine bonds (Fig. 4, B and C), which is a similar value to the original UTS of Neat-ABS films (Fig. 2E). Furthermore, the transverse-printed part of ALD-33 visibly showed better interlayer integration as indicated by smoother edge and interlayer joints, whereas the Neat-ABS printout displayed curvatures at the edge by the printing path and sharp topological valleys at the interlayer joint (Fig. 4G and fig. S15). Thus, dynamic cross-linking in the ABS-vitrimer without postprocessing creates strong interfilament interfaces, which is typically limited to 3D printing of thermosets with postextrusion cross-linking (*23*). Furthermore, the option to post-anneal the vitrimer samples is also available to further enhance the interlayer strength or reduce scratches on surfaces (fig. S16). We also examined the solvent resistance of specimens immersed in THF to corroborate the cross-linking throughout the layered structure (Fig. 4H and fig. S17). Despite some swelling, the ABS-vitrimer maintained the printed structure well and exhibited insignificant mass loss, whereas the Neat-ABS disintegrated within 1 hour. This solvent stability thereby supports that interlayer covalent bonds preserve the layered structure to resist disintegration. Moreover, this solvent resistance enables easy separation of ABS-vitrimer from its waste mixtures with Neat-ABS or other soluble plastics (e.g., Styrofoam) via a simple dissolution-decanting procedure (Fig. 4I). Thus, ABS-vitrimer can be separated and readily recycled, and dissolved Neat-ABS waste can be again upcycled to ABS-vitrimer (Figs. 1 and 2 and fig. S1). Alternatively, we can also decross-link and dissolve the ABS-vitrimer on demand by adding an excess amount of monofunctional amines (e.g., octylamine) (*29*, *32*), which provides another possible solution-based separation path (fig. S18).

Furthermore, even when mixed with Neat-ABS, the used ABS-vitrimer could be directly reprinted using the same printing protocols (Fig. 4J and fig. S19). The discarded ABS-vitrimer wastes were fragmented into extruder-feedable sizes and then extruded into recycled filaments. The vitrimer wastes could be mixed with Neat-ABS wastes to form blends to control the amount and color of printouts. The reusability and compatibility of ABS-vitrimer with Neat-ABS thus attest that wastes of Neat-ABS, ABS-vitrimer, and

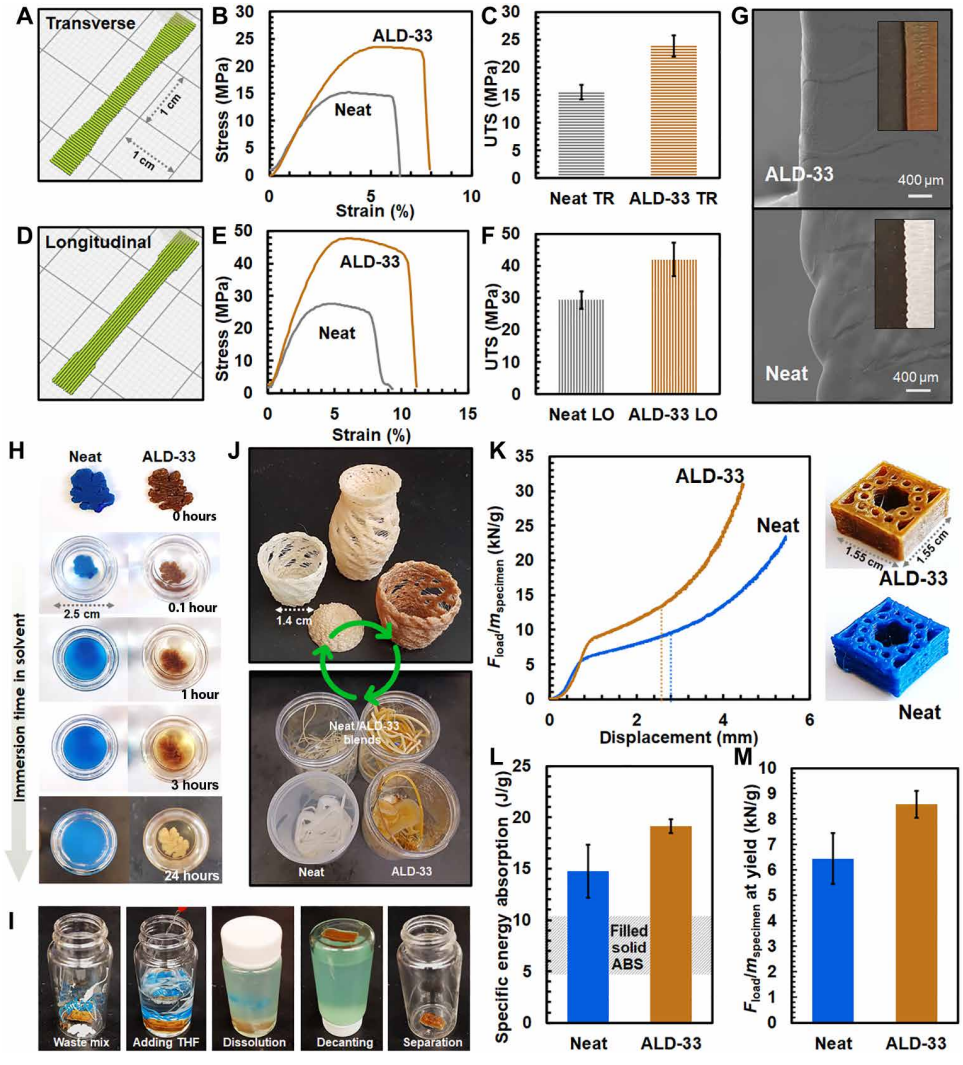

Fig. 4. FFF of ABS-vitrimers. (**A**) Computer-aided design (CAD) of a single-layered dog-bone tensile specimen printed in the transverse path. (**B**) Tensile stress-strain curves and (**C**) UTS of transverse-printed specimens made of Neat-ABS and ALD-33. (**D**) The CAD, (**E**) the tensile stress-strain curves, and (**F**) the UTS of longitudinal-printed specimens. (**G**) Scanning electron microscopy (SEM) images showing edges of the transverse-printed specimens. (**H**) Solvent resistance of an FFF-printed oak leaf structure (0.3 g) over 24 hours in THF (10 ml) at room temperature. The blue Neat-ABS was used for better visual comparison. (**I**) Separation of ABS-vitrimer from its unsorted waste mixture with Neat-ABS and Styrofoam by dissolution in THF followed by decanting. (**J**) The wastes of Neat-ABS, ABS-vitrimer, or their blends upcycled into 3D-printed baskets with different colors by iterating the same FFF protocols. (**K**) The compressive force-displacement curves of the unit mass ($F_{load}/m_{specimen}$) of beetles' forewing–inspired structures printed from Neat-ABS and ALD-33. (**L**) Specific energy absorption (SEA) and (**M**) the yielding $F_{load}/m_{specimen}$ at the displacement of ~0.4 mm in (K). The shaded area indicates the typical SEA range of a fully filled structure of Neat-ABS. The error bars indicate SDs from triplicate measurements.

unsorted mixtures produced during any step can be upcycled into useful and complex 3D structures difficult to obtain using conventional molding or casting methods such as baskets shown in Fig. 4J, instead of being discarded.

We reckon that the short time scale of bond rearrangements (τ), high E_a, and deformability obtained from the rational network design make the cross-linked ABS-vitrimer (re)printable and quickly develop interlayer bonding upon deposition of melts. These parameters shared in this study can serve as useful evaluators for implementing the direct FFF (re)printability (table S10) to other existing upcycled vitrimers (*19*) or future vitrimers. For example, compared with a previously reported epoxy vitrimer (*45*), ABS-vitrimer has ~1000 times shorter τ, ~3 times greater E_a, and deformability for direct FFF (re)processing/printing and in situ interlayer integration (table S11). Thus, upcycling ABS or other commodity thermoplastics to FFF-(re)printable vitrimers can be enabled by tuning these design parameters to emulate the thermomechanical properties of the untreated thermoplastics (tables S5 and S6). Although it is difficult to find examples of direct FFF of vitrimer comparable to engineering plastics, the ~40 MPa UTS of the ABS-vitrimer exceeds those of vitrimers applied in different extrusion-based AM, such as DIW (*27*). Another advantage of ABS-vitrimer FFF resides in the realization of intricate 3D geometries with superior structural mechanical properties. For example, bioinspired honeycomb structures of beetles' forewings, which are known for their excellent compressive properties (*46*), were facilely printed by FFF of ABS and ABS-vitrimer (Fig. 4K). The beetle-inspired ABS-vitrimer printout withheld higher load and absorbed more energy upon deformation [i.e., specific

energy absorption (SEA)] than the Neat-ABS. Notably, the SEA of ABS-vitrimer printout reached values as high as those of epoxy composites with chopped carbon fibers, which is threefold greater than those reported for filled structures of unmodified ABS (Fig. 4, K to M, and figs. S20 to S22) (*47*). The superior SEA obtained by bioinspired printing of upcycled ABS-vitrimer, therefore, indicates a path to achieve enhanced structural strength with substantially reduced material consumption compared with traditional manufacturing routes.

Last, we assessed the generality of our upcycling pathway of ABS-vitrimer using alternative cross-linkers of acetylacetate (AcAc) functional groups to form vinylogous urethanes by dynamic transamination (figs. S6 and S23 to S28) (*48*, *49*). To our satisfaction, the UTS and solvent resistance were enhanced to a similar level reached by ALD-33, proving our synthetic approach indeed can be versatilely applied to different cross-linking paths to enhance mechanical and chemical robustness (figs. S6 and S28). As exemplified by the AcAc systems, our thiol-ene click modification strategy for developing vitrimers can be greatly expanded material selections of different base polymers with alkene groups, branching molecules, and cross-linkers with diverse length, structure, and exchange groups to control material properties. This study thus provides a platform for developing other FFF-printable vitrimer and vitrimer composites for foreseeable applications ranging from electronics, vehicles, and robotics to biomedical therapeutics (*50*–*52*).

DISCUSSION

Our findings here offer an opening model to upcycle plastic wastes into elaborate 3D-printed structures of robust, recyclable cross-linked materials, and the strategy should be especially applicable to various currently printable commodity thermoplastics (*39*). The facile upcycling from existing commodity thermoplastics and the manufacturability of complex objects, such as beetle-inspired structures, enable multiple value-enhancing circular models. The design and evaluation of the ABS-vitrimer for the full FFF printing shared in this work present a tangible example to benchmark and apply FFF printability without modifying approachable printing protocols and conditions to the broad range of existing or future vitrimer materials. The approach of upcycling commodity plastics into materials with higher-value structures and properties through an accessible AM technique provides an imminently adoptable and pragmatic strategy toward establishing closed-loop circular manufacturing.

MATERIALS AND METHODS

Materials

ABS (molar mass of 211.3 g/mol) polymer pellets were purchased from 3DXTECH (Michigan, USA). Cysteamine, azobisisobutyronitrile (AIBN), glutaraldehyde, and octylamine were purchased from Sigma-Aldrich. All solvents used in this study including ethanol, THF, acetone, DCM, chloroform, and DMF were reagent grade purchased from Sigma-Aldrich. All chemical ingredients were purchased from Sigma-Aldrich unless specified otherwise.

Synthesis of ABS-vitrimers

The virgin or discarded ABS pellets were dissolved in a minimal amount of THF, and then the butadiene segments were functionalized with amine groups via thiol-ene reaction (*39*, *40*, *53*) triggered by adding cysteamine of more than 5× the molar equivalent amount to ethylene fractions in ABS (18% measured by ^{1}H NMR; see fig. S2 for more details) and AIBN as the radical initiator of 0.5× molar equivalent to the ethylene fraction in ABS following the reported method (*54*). The reaction proceeded at 60°C for 18 hours or longer with continuous stirring. The reaction was halted by cooling the reaction mixture to room temperature, and then the THF was removed via rotary vaporization. The product was then purified by precipitating in ethanol three times. The precipitates were obtained by decanting and filtering and then dried under vacuum at room temperature overnight. The products were characterized with ^{1}H NMR to quantify the amine-functionalized molar fraction (14 mol %) (fig. S2). The products were then mixed with glutaraldehyde or AcAc cross-linkers with desired ratios (i.e., different [—CHO]/[—NH_2]) in THF. The reaction continued longer than 5 hours at room temperature under continuous stirring. Then, the solvent was removed by vacuum, and the cross-linked product was further cured in a vacuum oven at 150°C for longer than 3 hours.

Synthesis of AcAc cross-linkers

For the synthesis of AcAc cross-linkers, please see the Supplementary Materials (figs. S23 to S26).

Spectroscopic characterizations

^{1}H NMR spectra were recorded with a Bruker Avance III 400 NMR spectrometer (400 MHz) (Massachusetts, USA) on the sample dissolved in THF-d_8 or $CDCl_3$ and analyzed with Bruker TopSpin software version 4.0.9 with the reference of THF-d_8 or $CDCl_3$ as the solvent. FTIR spectra were recorded with the Thermo Fisher Scientific Nicolet iS50 FTIR spectrometer (Massachusetts, USA) using the transmission mode on polymer film samples. The ^{13}C NMR spectra were collected on a Varian VNMRS spectrometer (California, USA) operating at 700 MHz ^{1}H frequency using a 3.2-mm T3 triple resonance Varian probe. The spectra were collected using a standard echo experiment at 22.5-kHz magic angle spinning rate (srate) with ^{1}H decoupling. The echo time was 1/srate. The spectra were collected with a recycle delay of 100 s with ~2000 scans.

Tensile analysis

Tensile stress-strain curves were obtained by using an Instron 3343 Universal Testing System (Massachusetts, USA) with a 1-kN load cell following the ASTM D1708 standard. Samples were prepared by hot pressing (0.7 metric ton) at 150°C for 30 min to make a film followed by punching to cut the dog-bone films with a total length of 18 mm, a gauged length of 7.0 mm, a gauged width of 2.52 mm, and an average thickness of 0.20 mm. For the tensile tests of 3D-printed specimens, please refer to the "FFF 3D printing" section. The samples were tested at room temperature. Samples were elongated at the rate of 1 mm/s until failure. Toughness was calculated from the area under the stress-strain curve. The mechanical properties were reported from the average of at least three specimens for each sample.

Dynamic mechanical analysis

Dynamic mechanical property analyses were carried out by TA Instruments DMA 850 System (Delaware, USA) by using a film tension clamp. The same dog-bone films used in the tensile analysis were used for characterization. Samples were tested at temperatures ranging from 35° to 130°C at a ramp rate of 3°C/min, with a frequency of 1 Hz and an amplitude of 20 μm.

Differential scanning calorimetry

The differential scanning calorimetry (DSC) analysis was performed using TA Instruments Q1000 DSC (Delaware, USA). Approximately 5 mg of samples was measured into standard sealed aluminum T-Zero pans. A heating cycle was then run from 25° to 200°C at a heating rate of 10°C/min under nitrogen with a 5-min isotherm at the maximum and minimum temperature. The specimens were subjected to three heating cycles.

Thermogravimetric analysis

The thermogravimetric analysis (TGA) was performed for assessing the thermal decomposition. The ~10 mg of sample was prepared and run from room temperature to 800°C at a heating rate of 10°C/min under nitrogen on a TA Instruments Q-50 TGA (Delaware, USA).

Rheological measurements

Rheological measurements were performed with a TA Instruments AR2000ex rheometer (Delaware, USA) using 4-mm aluminum parallel-plate geometry. For frequency sweep and stress relaxation experiments, the samples were tested at temperatures of 130°, 140°, 150°, 160°, and 170°C by applying a constant strain at 1%. The frequency sweep tests were performed at a 0.1- to 100-rad/s frequency range and then processed through time-temperature superposition to generate master curves at a reference temperature of 150°C via TA Instrument TRIOS software by using the Williams-Landel-Ferry equation (table S4). The relaxation modulus $G(t)$ (Pa) was recorded up to 1000 s at a constant temperature. The τ (s) were determined following the widely used custom to evaluate stress relaxation of vitrimers as the time when $G(t)/G_i$ became 1/e (~36.8%) from the Maxwell model (Eq. 1), where G_i (Pa) is the modulus at time 0.1 s when the strain was stabilized at the set value

$$G(t) = G_i \exp\left(-\frac{t}{\tau}\right) \quad (1)$$

The creep test was performed at 130°, 140°, 150°, and 160°C at a constant stress of 50,000 Pa. Before each rheological measurement, the sample underwent thermal equilibration for 5 min. The temperature dependence of obtained τ was fitted with the following Arrhenius relation (Eq. 2) (*36*, *48*, *55*)

$$\tau(T) = \tau_0 \exp\left(\frac{E_a}{RT}\right) \quad (2)$$

where $\tau(T)$ is the relaxation time (s) measured at temperature T (K), τ_0 is the characteristic relaxation time at infinite temperature (s, Arrhenius prefactor), E_a is the apparent activation energy (J/mol), and R is the ideal gas constant (J/mol·K).

Chemical-solvent resistance test

The chemical resistance of the samples was tested by immersing each sample in more than 30 times the volume of acetone, THF, chloroform, DCM, or DMF at room temperature. The dissolution was visually observed and compared within 24 hours unless specified otherwise. When separating the ABS-vitrimer from unsorted plastic waste mixtures, THF was used to dissolve the dissolvable plastics followed by decanting the supernatant solution.

Fabrication of polymer filaments

The polymer filaments were produced and spooled by using the Filabot Ex2 Extruder and Spooler System (Vermont, USA). The polymer pellets or particles were fed into the hopper and extruded at 230°C through a 1.75-mm die nozzle. The formed filament was wound onto a spool by using the spooler at ambient temperature (fig. S13). The extrusion and winding rates were adjusted to stably produce the 1.75-mm-thick filament wound onto a spool.

FFF 3D printing

The FFF 3D printing was performed using a Hyrel 3D System 30M (Georgia, USA). The 1.75-mm polymer filaments were loaded into the filament feeder of the printer and continuously fed during printing. The polymer was extruded at 230°C, the typical extrusion temperature of ABS through a 0.5-mm hothead nozzle and deposited onto the hotbed stage. The hotbed stage temperature was 90° to 100°C. The printing infill pattern was designed to print single-layered tensile dog-bone specimens that were 0.2× size of ASTM D638 type I (i.e., full length of 33 mm, gauged width of 3.0 mm, grip width of 4 mm, and thickness of 0.5 mm) in either transverse or longitudinal paths of printed layers (fig. S14). The corresponding G-code was coded via Ultimaker Cura software version 4.7.1 and was used to print Neat-ABS and ABS-vitrimers. The deposited samples were carefully retrieved after 5 min without any postmodification. The 3D-printed tensile specimens were subjected to the aforementioned tensile test conditions. Likewise, the same G-codes and printing parameters for other printout structures were used to print Neat-ABS, ABS-vitrimer, or their mixtures.

Scanning electron microscopy

The surface morphological properties of 3D-printed samples were characterized by a Zeiss Auriga focused ion beam–scanning electron microscopy (SEM) system (Germany). All samples were sputter-coated with gold for 10 s before imaging, and images were obtained with an operating voltage of 5 kV.

Compression test

The compression tests were performed at ambient conditions by using an MTS 808 electromechanical testing machine (Minnesota, USA) and a die-set fixture at a constant crosshead displacement rate of 20 μm/s. The compression specimens were printed in cuboid structure (width by length by thickness: 15.5 mm by 15.5 mm by 5 to 7 mm, 1.0 to 1.5 g) with cross-sectional geometry inspired by the honeycomb structures of beetles' forewings (*56*). The SEA that estimates the ability of a unit mass of a material to dissipate crushing energy through plastic deformation is defined as follows

$$\mathrm{SEA} = \int_0^{d_{max}} \frac{F(x)}{m} dx \quad (3)$$

where m is the mass of the energy-absorbing material (g), $F(x)$ is the compressive force [i.e., load (kN)] at the displacement x (mm), and d_{max} is the maximum displacement (mm) before material densification where the slope of $F(x)$ surges at a later stage. See figs. S20 to S22 for more details.

SUPPLEMENTARY MATERIALS

Supplementary material for this article is available at https://science.org/doi/10.1126/sciadv.abn6006

View/request a protocol for this paper from *Bio-protocol*.

REFERENCES AND NOTES

1. A. Stubbins, K. L. Law, S. E. Muñoz, T. S. Bianchi, L. Zhu, Plastics in the Earth system. *Science* **373**, 51–55 (2021).

2. E. Macarthur, Beyond plastic waste. *Science* **358**, 843–843 (2017).
3. M. Häußler, M. Eck, D. Rothauer, S. Mecking, Closed-loop recycling of polyethylene-like materials. *Nature* **590**, 423–427 (2021).
4. P. R. Christensen, A. M. Scheuermann, K. E. Loeffler, B. A. Helms, Closed-loop recycling of plastics enabled by dynamic covalent diketoenamine bonds. *Nat. Chem.* **11**, 442–448 (2019).
5. N. Vora, P. R. Christensen, J. Demarteau, N. R. Baral, J. D. Keasling, B. A. Helms, C. D. Scown, Leveling the cost and carbon footprint of circular polymers that are chemically recycled to monomer. *Sci. Adv.* **7**, eabf0187 (2021).
6. J. Zheng, S. Suh, Strategies to reduce the global carbon footprint of plastics. *Nat. Clim. Change* **9**, 374–378 (2019).
7. R. Meys, A. Kätelhön, M. Bachmann, B. Winter, C. Zibunas, S. Suh, A. Bardow, Achieving net-zero greenhouse gas emission plastics by a circular carbon economy. *Science* **374**, 71–76 (2021).
8. S. R. Nicholson, N. A. Rorrer, A. C. Carpenter, G. T. Beckham, Manufacturing energy and greenhouse gas emissions associated with plastics consumption. *Joule* **5**, 673–686 (2021).
9. L. T. Korley, T. H. Epps, B. A. Helms, A. J. Ryan, Toward polymer upcycling—Adding value and tackling circularity. *Science* **373**, 66–69 (2021).
10. Y. Y. C. Choong, H. W. Tan, D. C. Patel, W. T. N. Choong, C.-H. Chen, H. Y. Low, M. J. Tan, C. D. Patel, C. K. Chua, The global rise of 3D printing during the COVID-19 pandemic. *Nat. Rev. Mater.* **5**, 637–639 (2020).
11. S. Carr, What is Additive Manufacturing? (Office of Energy Efficiency & Renewable Energy, 2017); https://energy.gov/eere/articles/what-additive-manufacturing#1.
12. A. R. Rahimi, J. M. Garciá, Chemical recycling of waste plastics for new materials production. *Nat. Rev. Chem.* **1**, 0046 (2017).
13. S. C. Ligon, R. Liska, J. Stampfl, M. Gurr, R. Mülhaupt, Polymers for 3D printing and customized additive manufacturing. *Chem. Rev.* **117**, 10212–10290 (2017).
14. S. A. M. Tofail, E. P. Koumoulos, A. Bandyopadhyay, S. Bose, L. O'Donoghue, C. Charitidis, Additive manufacturing: Scientific and technological challenges, market uptake and opportunities. *Mater. Today* **21**, 22–37 (2018).
15. "Worldwide most used 3D printing technologies, as of July 2018*," (Statista, 2020); https://statista.com/statistics/756690/worldwide-most-used-3d-printing-technologies/.
16. P. Chesser, B. Post, A. Roschli, C. Carnal, R. Lind, M. Borish, L. Love, Extrusion control for high quality printing on Big Area Additive Manufacturing (BAAM) systems. *Addit. Manuf.* **28**, 445–455 (2019).
17. E. N. Peters, *Plastics: Thermoplastics, Thermosets, and Elastomers* (Wiley-Interscience, 2002).
18. D. Montarnal, M. Capelot, F. Tournilhac, L. Leibler, Silica-like malleable materials from permanent organic networks. *Science* **334**, 965–968 (2011).
19. M. Röttger, T. Domenech, R. van der Weegen, A. Breuillac, R. Nicolaÿ, L. Leibler, High-performance vitrimers from commodity thermoplastics through dioxaborolane metathesis. *Science* **356**, 62–65 (2017).
20. N. J. Van Zee, R. Nicolaÿ, Vitrimers: Permanently crosslinked polymers with dynamic network topology. *Prog. Polym. Sci.* **104**, 101233 (2020).
21. J. R. Davidson, G. A. Appuhamillage, C. M. Thompson, W. Voit, R. A. Smaldone, Design paradigm utilizing reversible Diels–Alder reactions to enhance the mechanical properties of 3D printed materials. *ACS Appl. Mater. Interfaces* **8**, 16961–16966 (2016).
22. G. A. Appuhamillage, J. C. Reagan, S. Khorsandi, J. R. Davidson, W. Voit, R. A. Smaldone, 3D printed remendable polylactic acid blends with uniform mechanical strength enabled by a dynamic Diels–Alder reaction. *Polym. Chem.* **8**, 2087–2092 (2017).
23. K. Yang, J. C. Grant, P. Lamey, A. Joshi-Imre, B. R. Lund, R. A. Smaldone, W. Voit, Diels-Alder reversible thermoset 3D printing: Isotropic thermoset polymers via fused filament fabrication. *Adv. Funct. Mater.* **27**, 1700318 (2017).
24. M. Nadgorny, J. Collins, Z. Xiao, P. J. Scales, L. A. Connal, 3D-printing of dynamic self-healing cryogels with tuneable properties. *Polym. Chem.* **9**, 1684–1692 (2018).
25. M. Nadgorny, Z. Xiao, L. A. Connal, 2D and 3D-printing of self-healing gels: Design and extrusion of self-rolling objects. *Mol. Syst. Des. Eng.* **2**, 283–292 (2017).
26. W. Niu, Z. Zhang, Q. Chen, P.-F. Cao, R. C. Advincula, Highly recyclable, mechanically isotropic and healable 3D-printed elastomers via polyurea vitrimers. *ACS Mater. Lett.* **3**, 1095–1103 (2021).
27. Q. Shi, K. Yu, X. Kuang, X. Mu, C. K. Dunn, M. L. Dunn, T. Wang, H. Jerry Qi, Recyclable 3D printing of vitrimer epoxy. *Mater. Horizons* **4**, 598–607 (2017).
28. P. Taynton, K. Yu, R. K. Shoemaker, Y. Jin, H. J. Qi, W. Zhang, Heat- or water-driven malleability in a highly recyclable covalent network polymer. *Adv. Mater.* **26**, 3938–3942 (2014).
29. P. Taynton, H. Ni, C. Zhu, K. Yu, S. Loob, Y. Jin, H. J. Qi, W. Zhang, Repairable woven carbon fiber composites with full recyclability enabled by malleable polyimine networks. *Adv. Mater.* **28**, 2904–2909 (2016).
30. S. Dhers, G. Vantomme, L. Avérous, A fully bio-based polyimine vitrimer derived from fructose. *Green Chem.* **21**, 1596–1601 (2019).
31. S. Wang, S. Ma, Q. Li, W. Yuan, B. Wang, J. Zhu, Robust, fire-safe, monomer-recovery, highly malleable thermosets from renewable bioresources. *Macromolecules* **51**, 8001–8012 (2018).
32. X. Lei, Y. Jin, H. Sun, W. Zhang, Rehealable imide–imine hybrid polymers with full recyclability. *J. Mater. Chem. A* **5**, 21140–21145 (2017).
33. Z. Zhou, X. Su, J. Liu, R. Liu, Synthesis of vanillin-based polyimine vitrimers with excellent reprocessability, fast chemical degradability, and adhesion. *ACS Appl. Polym. Mater.* **2**, 5716–5725 (2020).
34. Y. Liu, Z. Tang, J. Chen, J. Xiong, D. Wang, S. Wang, S. Wu, B. Guo, Tuning the mechanical and dynamic properties of imine bond crosslinked elastomeric vitrimers by manipulating the crosslinking degree. *Polym. Chem.* **11**, 1348–1355 (2020).
35. B. R. Elling, W. R. Dichtel, Reprocessable cross-linked polymer networks: Are associative exchange mechanisms desirable? *ACS Cent. Sci.* **6**, 1488–1496 (2020).
36. G. M. Scheutz, J. J. Lessard, M. B. Sims, B. S. Sumerlin, Adaptable crosslinks in polymeric materials: Resolving the intersection of thermoplastics and thermosets. *J. Am. Chem. Soc.* **141**, 16181–16196 (2019).
37. S. H. Ahn, M. Montero, D. Odell, S. Roundy, P. K. Wright, Anisotropic material properties of fused deposition modeling ABS. *Rapid Prototyp. J.* **8**, 248–257 (2002).
38. I. Vollmer, M. J. Jenks, M. C. Roelands, R. J. White, T. van Harmelen, P. de Wild, G. P. van Der Laan, F. Meirer, J. T. Keurentjes, B. M. Weckhuysen, Beyond mechanical recycling: Giving new life to plastic waste. *Angew. Chem. Int. Ed.* **59**, 15402–15423 (2020).
39. A. B. Lowe, Thiol–ene "click" reactions and recent applications in polymer and materials synthesis: A first update. *Polym. Chem.* **5**, 4820–4870 (2014).
40. C. E. Hoyle, C. N. Bowman, Thiol–ene click chemistry. *Angew. Chem. Int. Ed.* **49**, 1540–1573 (2010).
41. K. S. Erokhin, E. G. Gordeev, V. P. Ananikov, Revealing interactions of layered polymeric materials at solid-liquid interface for building solvent compatibility charts for 3D printing applications. *Sci. Rep.* **9**, 20177 (2019).
42. M. L. Shofner, K. Lozano, F. J. Rodríguez-Macías, E. V. Barrera, Nanofiber-reinforced polymers prepared by fused deposition modeling. *J. Appl. Polym. Sci.* **89**, 3081–3090 (2003).
43. C. A. Angell, Formation of glasses from liquids and biopolymers. *Science* **267**, 1924–1935 (1995).
44. Y. Yang, S. Zhang, X. Zhang, L. Gao, Y. Wei, Y. Ji, Detecting topology freezing transition temperature of vitrimers by AIE luminogens. *Nat. Commun.* **10**, 3165 (2019).
45. A. Ruiz De Luzuriaga, R. Martin, N. Markaide, A. Rekondo, G. Cabañero, J. Rodríguez, I. Odriozola, Epoxy resin with exchangeable disulfide crosslinks to obtain reprocessable, repairable and recyclable fiber-reinforced thermoset composites. *Mater. Horizons* **3**, 241–247 (2016).
46. N. San Ha, G. Lu, A review of recent research on bio-inspired structures and materials for energy absorption applications. *Compos. B Eng.* **181**, 107496 (2020).
47. G. C. Jacob, J. M. Starbuck, J. F. Fellers, S. Simunovic, Energy absorption in chopped carbon fiber epoxy composites for automotive crashworthiness. *Polym. J.* **35**, 560–567 (2003).
48. W. Denissen, G. Rivero, R. Nicolaÿ, L. Leibler, J. M. Winne, F. E. Du Prez, Vinylogous urethane vitrimers. *Adv. Funct. Mater.* **25**, 2451–2457 (2015).
49. W. Denissen, M. Droesbeke, R. Nicolaÿ, L. Leibler, J. M. Winne, F. E. Du Prez, Chemical control of the viscoelastic properties of vinylogous urethane vitrimers. *Nat. Commun.* **8**, 14857 (2017).
50. Y. Yang, Y. Xu, Y. Ji, Y. Wei, Functional epoxy vitrimers and composites. *Prog. Mater. Sci.* **120**, 100710 (2020).
51. S. Kim, A. U. Regitsky, J. Song, J. Ilavsky, G. H. McKinley, N. Holten-Andersen, In situ mechanical reinforcement of polymer hydrogels via metal-coordinated crosslink mineralization. *Nat. Commun.* **12**, 667 (2021).
52. C. S. O'Bryan, T. Bhattacharjee, S. Hart, C. P. Kabb, K. D. Schulze, I. Chilakala, B. S. Sumerlin, W. G. Sawyer, T. E. Angelini, Self-assembled micro-organogels for 3D printing silicone structures. *Sci. Adv.* **3**, e1602800 (2017).
53. D. P. Nair, M. Podgórski, S. Chatani, T. Gong, W. Xi, C. R. Fenoli, C. N. Bowman, The Thiol-Michael addition click reaction: A powerful and widely used tool in materials chemistry. *Chem. Mater.* **26**, 724–744 (2013).
54. L. M. Campos, K. L. Killops, R. Sakai, J. M. Paulusse, D. Damiron, E. Drockenmuller, B. W. Messmore, C. J. Hawker, Development of thermal and photochemical strategies for thiol– Ene click polymer functionalization. *Macromolecules* **41**, 7063–7070 (2008).
55. W. Denissen, J. M. Winne, F. E. Du Prez, Vitrimers: Permanent organic networks with glass-like fluidity. *Chem. Sci.* **7**, 30–38 (2016).
56. P. Hao, J. Du, Energy absorption characteristics of bio-inspired honeycomb column thin-walled structure under impact loading. *J. Mech. Behav. Biomed. Mater.* **79**, 301–308 (2018).
57. Mission Possible: Reaching net-zero carbon emissions from harder-to-abate sectors by mid-century. Sectoral Focus Plastics (Energy Transitions Commission, 2018); https://energy-transitions.org/wp-content/uploads/2020/08/ETC-sectoral-focus-Plastics_final.pdf.

58. A. Zhakeyev, P. Wang, L. Zhang, W. Shu, H. Wang, J. Xuan, Additive manufacturing: Unlocking the evolution of energy materials. *Adv. Sci.* **4**, 1700187 (2017).
59. P. F. Britt, G. W. Coates, K. I. Winey, J. Byers, E. Chen, B. Coughlin, C. Ellison, J. Garcia, A. Goldman, J. Guzman, "Report of the Basic Energy Sciences Roundtable on Chemical Upcycling of Polymers," (U.S. DOE Office of Science (SC), 2019).
60. "Plastics, the Circular Economy and Global Trade," (World Economic Forum, 2020); www3.weforum.org/docs/WEF_Plastics_the_Circular_Economy_and_Global_Trade_2020.pdf.
61. R. L. Truby, J. A. Lewis, Printing soft matter in three dimensions. *Nature* **540**, 371–378 (2016).
62. "3D Printing Market Size, Share & COVID-19 Impact Analysis, By Component (Hardware, Software, Services), By Technology (FDM, SLS, SLA, DMLS/SLM, Poly jet, Multi Jet Fusion, DLP, Binder Jetting, EBM, CLIP/CDLP, SDL, LOM), By Application (Prototyping, Production, Proof of Concept, Others), By End User (Automotive, Aerospace, and Defense, Healthcare, Architecture and Construction, Consumer Products, Education, Others) and Regional Forecast, 2021–2028," (Fortune Business Insights, 2021); https://fortunebusinessinsights.com/industry-reports/3d-printing-market-101902.
63. I. Campbell, O. Diegel, J. Kowen, T. Wohlers, *Wohlers Report 2018: 3D Printing and Additive Manufacturing State of the Industry: Annual Worldwide Progress Report* (Wohlers Associates, 2018).
64. "Which 3D printing technologies do you use?," (Statista, 2021); https://statista.com/statistics/560304/worldwide-survey-3d-printing-top-technologies/.
65. V. Kishore, C. Ajinjeru, A. Nycz, B. Post, J. Lindahl, V. Kunc, C. Duty, Infrared preheating to improve interlayer strength of big area additive manufacturing (BAAM) components. *Addit. Manuf.* **14**, 7–12 (2017).
66. "Production capacity of acrylonitrile butadiene styrene worldwide from 2013 to 2023," (Statista, 2019); https://statista.com/statistics/856670/acrylonitrile-butadiene-styrene-global-production-capacity/.
67. "Engineering Plastics Market Report," (Ceresana, 2018); https://ceresana.com/en/market-studies/plastics/engineering-plastics/.
68. W. Zou, J. Dong, Y. Luo, Q. Zhao, T. Xie, Dynamic Covalent Polymer Networks: From old chemistry to modern day innovations. *Adv. Mater.* **29**, 1606100 (2017).
69. Z. C. Eckel, C. Zhou, J. H. Martin, A. J. Jacobsen, W. B. Carter, T. A. Schaedler, Additive manufacturing of polymer-derived ceramics. *Science* **351**, 58–62 (2016).
70. X. Zheng, H. Lee, T. H. Weisgraber, M. Shusteff, J. DeOtte, E. B. Duoss, J. D. Kuntz, M. M. Biener, Q. Ge, J. A. Jackson, S. O. Kucheyev, N. X. Fang, C. M. Spadaccini, Ultralight, ultrastiff mechanical metamaterials. *Science* **344**, 1373–1377 (2014).
71. Z. Qin, B. G. Compton, J. A. Lewis, M. J. Buehler, Structural optimization of 3D-printed synthetic spider webs for high strength. *Nat. Commun.* **6**, 7038 (2015).
72. B. G. Compton, J. A. Lewis, 3D-printing of lightweight cellular composites. *Adv. Mater.* **26**, 5930–5935 (2014).
73. J. K. Wilt, D. Gilmer, S. Kim, B. G. Compton, T. Saito, Direct ink writing techniques for in situ gelation and solidification. *MRS Commun.* **11**, 106–121 (2021).
74. Q. Chen, L. Han, J. Ren, L. Rong, P. Cao, R. C. Advincula, 4D printing via an unconventional fused deposition modeling route to high-performance thermosets. *ACS Appl. Mater. Interfaces* **12**, 50052–50060 (2020).
75. T. Fujisawa, B. Rubin, A. Suzuki, P. S. Patel, W. A. Gahl, B. H. Joshi, R. K. Puri, Cysteamine suppresses invasion, metastasis and prolongs survival by inhibiting matrix metalloproteinases in a mouse model of human pancreatic cancer. *PLOS ONE* **7**, e34437 (2012).
76. R. K. J. Puri, Bharatkumar, *Use of Cysteamine to Treat Metastatic Cancer* (U.S. Food & Drug Administration (FDA), 2018); https://fda.gov/science-research/licensing-and-collaboration-opportunities/use-cysteamine-treat-metastatic-cancer.
77. G. Devereux, D. Fraser-Pitt, J. Robertson, E. Devlin, D. Mercer, D. O'Neil, Cysteamine as a future intervention in cystic fibrosis against current and emerging pathogens: A patient-based ex vivo study confirming its antimicrobial and mucoactive potential in sputum. *EBioMedicine* **2**, 1507–1512 (2015).
78. World Health Organization, "World Health Organization model list of essential medicines: 21st list 2019," (World Health Organization, Geneva, 2019); https://apps.who.int/iris/handle/10665/325771.
79. "FDA-Cleared Sterilants and High Level Disinfectants with General Claims for Processing Reusable Medical and Dental Devices," (U.S. Food & Drug Administration (FDA), 2019); https://fda.gov/medical-devices/reprocessing-reusable-medical-devices-information-manufacturers/fda-cleared-sterilants-and-high-level-disinfectants-general-claims-processing-reusable-medical-and.
80. N. Peez, W. Imhof, Quantitative ^{1}H-NMR spectroscopy as an efficient method for identification and quantification of PVC, ABS and PA microparticles. *Analyst* **145**, 5363–5371 (2020).
81. N. T. Thanh Truc, B. K. Lee, Selective separation of ABS/PC containing BFRs from ABSs mixture of WEEE by developing hydrophilicity with ZnO coating under microwave treatment. *J. Hazard. Mater.* **329**, 84–91 (2017).
82. "IR Spectrum Table & Chart," (Sigma-Aldrich Inc., 2021); https://sigmaaldrich.com/US/en/technical-documents/technical-article/analytical-chemistry/photometry-and-reflectometry/ir-spectrum-table#table-by-group.
83. M. Senthilkumaran, L. Eswaran, C. Saravanan, P. Puthiaraj, P. Rameshkumar, P. M. Mareeswaran, Imine-linked polymer/silica composites for CO2 sequestration. *Mater. Chem. Phys.* **239**, 121995 (2020).
84. B. Zhang, K. Kowsari, A. Serjouei, M. L. Dunn, Q. Ge, Reprocessable thermosets for sustainable three-dimensional printing. *Nat. Commun.* **9**, 1831 (2018).
85. S. Szczepanik, P. Bednarczyk, Bending and compression properties of abs and pet structural materials printed using FDM technology. *J. Cast. Mater. Eng.* **1**, 39 (2017).
86. S. Brischetto, C. Ferro, P. Maggiore, R. Torre, Compression tests of ABS specimens for UAV components produced via the FDM technique. *Dent. Tech.* **5**, 20 (2017).

Acknowledgments: We thank C. Bowland for the initial trial on a compression test, and we thank J. Damron for conducting the solid-state NMR experiment. This manuscript has been authored by UT-Battelle LLC under contract DE-AC05-00OR22725 with the U.S. Department of Energy (DOE). The U.S. government retains, and the publisher, by accepting the article for publication, acknowledges that the U.S. government retains a nonexclusive, paid-up, irrevocable, worldwide license to publish or reproduce the published form of this manuscript, or allow others to do so, for U.S. government purposes. DOE will provide public access to these results of federally sponsored research in accordance with the DOE Public Access Plan (http://energy.gov/downloads/doe-public-access-plan). **Funding:** This research was sponsored by the Laboratory Directed Research and Development Program of Oak Ridge National Laboratory managed by UT-Battelle LLC for the U.S. DOE. Solid-state NMR and dissolution experiments are supported by the U.S. DOE, Office of Science, Materials Sciences, and Engineering Division. **Author contributions:** T.S. and S.K. conceived this project. T.S. and S.K. designed, and S.K. performed the experiments including synthesis, processing, 3D printing, and characterizations. M.A.R. assisted and provided discussions on the design and practice of chemical synthesis. M.A. synthesized and provided the AcAc cross-linker molecules. D.B.G. performed DSC and TGA measurements and coordinated setting up the 3D printing and compressive mechanical analysis. B.L. performed DSC and SEM observations and provided initial help on using the filament extruder. J.K.W. provided discussions on setting up and executing 3D printing. E.L.-C. performed the compressive mechanical analysis and helped interpret its data. S.K. and T.S. wrote the manuscript. All authors read and commented on the manuscript. **Competing interests:** S.K., M.A.R., and T.S. are inventors on a patent application related to this work filed by USPTO (no. 63/277, 288, filed on 9 November 2021). The authors declare that they have no other competing interests. **Data and materials availability.** All data needed to evaluate the conclusions in this paper are present in the paper and/or the Supplementary Materials.

Submitted 7 December 2021
Accepted 18 April 2022
Published 3 June 2022
10.1126/sciadv.abn6006

ScienceAdvances

Closed-loop additive manufacturing of upcycled commodity plastic through dynamic cross-linking

Sungjin KimMd Anisur RahmanMd ArifuzzamanDustin B. GilmerBingrui LiJackson K. WiltEdgar Lara-CurzioTomonori Saito

Sci. Adv., 8 (22), eabn6006. • DOI: 10.1126/sciadv.abn6006

Science Advances (ISSN) is published by the American Association for the Advancement of Science. 1200 New York Avenue NW, Washington, DC 20005. The title *Science Advances* is a registered trademark of AAAS.